Measuring Coupling Coefficient of Windings With Dissimilar Turns' Number or Tight Coupling Using Resonance

David Gilabert-Palmer, Esteban Sanchis-Kilders, *Senior Member, IEEE*, Vicente Esteve, *Senior Member, IEEE*, Agustín Ferreres, Juan B. Ejea, Enrique Maset, *Member, IEEE*, José Jordn, *Senior Member, IEEE*, and Enrique Dede, *Member, IEEE*

***Abstract*—Multiple coupled inductors are used in power electronics to improve the dynamic cross regulation and to reduce mass and volume, mainly in high performance application, such as space or defense, where manufacturing cost is not the main driver. These elements can be modeled with its inductance matrix which is a symmetric and positive semidefinite matrix. The inductance matrix eases circuit analysis, many known circuital models are directly related to it and it can be used in SPICE simulation via its coupling coefficient component, which can be identified as the normalized matrix of the inductance matrix. Therefore, a precise and correct measurement technique of the inductance matrix or coupling coefficient matrix is needed. This paper analyzes different measuring techniques described in the technical literature and proposes a new method to measure the coupling coefficient or inductance matrix of tight coupled or dissimilar turns' number windings, where other methods fail. A discussion follows, to know the influence of parasitic elements in the accuracy of the new proposed method called resonance (RE) method. The paper adds three experimental examples to verify the theoretical study and concludes that the RE method provides correct values of the coupling coefficient k of tight coupled or dissimilar turns' number windings compared to other measurement techniques.**

***Index Terms*—Inductance measurements, inductors, magnetic devices, mutual coupling.**

I. Introduction

SWITCHING mode power supplies with multiple-outputs are widely employed. The use of multiple coupled inductors (MCI) is still a hot topic [1]–[5] in order to save volume, mass, reduce current ripple, improve dynamic cross regulation, and reduce EMI. Therefore, it is an important goal to have an accurate and easy to measure model of an MCI that helps to analyze the circuit and guarantees the simulation of the power converter.

Manuscript received July 27, 2017; revised October 23, 2017 and November 30, 2017; accepted January 3, 2018. Date of publication March 14, 2018; date of current version August 7, 2018. This work was supported by the Spanish Ministerio de Economa, Industria y Competitividad, through Projects ESP2013-47349-C6-5-R, ESP2014-56169-C6-4-R, and ESP2016-77548-C5-5-R, including a percentage from European FEDER funds. Recommended for publication by Associate Editor J. Acero. *(Corresponding author: Esteban Sanchis-Kilders.)*

The authors are with the Departamento de Ingeniería Electrónica/ETSE, Universitat of Valencia, Valencia 46100, Spain (e-mail: david.gilabert@uv.es; esteban.sanchis@uv.es; vesteveg@uv.es; ferreres@uv.es; Juan.B.Ejea@uv.es; enrique.maset@uv.es; jose.jordan@uv.es; enrique.dede@uv.es).

Color versions of one or more of the figures in this paper are available online at http://ieeexplore.ieee.org.

Digital Object Identifier 10.1109/TPEL.2018.2794621

A. Coupled Inductors Models

It is known that the inductance matrix allows us to describe complex inductors with multiple windings and the coupling between all of them. Many other models are based on approximations and reductions of the inductance matrix, that result in simple equivalent circuits.

Unfortunately, these approximations cannot always be applied to complex coupled inductors. Therefore, knowing the inductance matrix precisely allows either to use the inductance matrix for the mathematical circuit analysis or derivation of other existing models related to it like the cantilever model [6]. Of course, inductance matrix does not take into account second-order effects, such as parasitic capacitance and losses in the core and the windings, but it precisely describes the coupling between all the windings.

Other models, as described in [7]–[9], are used for transformers with two (or even three) windings. But it is difficult to add more windings to these models and they lose their simplicity and accuracy, because they neglect the cross coupling influence. For example, the π model is only useful for two windings as explained in [10].

Many of the models described in [8], [10]–[13] were proposed to determine the leakage (and magnetizing inductance) of the magnetic element, which is known to be responsible for voltage spikes and parasitic ringing during switching action. But it is very difficult to determine these parasitic elements and their influence for more than two windings (see [6]).

In [10], [12], and [13], the **H** field is studied (Ampere's law) and together with the geometry of the magnetic element and using the reluctance model, the leakage inductance is deduced. In [8], a more detailed study is done because it includes Eddy current losses and demonstrates that they affect the leakage inductance. Maxwell's equations are not only used in [8], but also in [14] and [15]. Geometry also plays an important role, but the dependence of the leakage with geometry in this paper makes it difficult to generalize the method to more complex structures.

In [16], coupled inductors are proposed to reduce losses and it shows a clear relation between the reluctance model and the inductance matrix.

Unfortunately, none of the previous described models can be easily generalized for many windings.

The cantilever model described in [6] is so far the most accurate generalized model as it considers "n" windings, and it uses circuital elements to describe the behavior of the MCI. It is not a reduced model and its relation to the inductance matrix is provided. In [6], another model is also presented that improves the convergence of the SPICE simulation when used for complex MCI.

B. Inductance Matrix Measurement

Therefore, the inductance matrix has been chosen as the preferred model to describe MCI because it not only provides easy circuit analysis capabilities, but almost all other models found in the literature are related to it.

The next step and the main objective of this paper is to measure correctly and accurately the elements of the inductance or coupling coefficient matrix. It is known that the inductance matrix is symmetric, with real and positive elements and as demonstrated in [17], it is also positive semidefinite (PSD). This also applies for the coupling coefficient matrix. But, the PSD condition is only necessary, thus we can have PSD inductance matrices that are not correct (this will be demonstrated later). In addition, under low coupling coefficient conditions, mutual inductances can change from positive to negative when changing the geometry of the system, as demonstrated in [18] and [19]. If geometry is maintained constant, like when using ferrite cores, and the dot convention (phasing) is taken into account, windings can be arranged in such a way that measured mutual inductance is always positive.

Among others, one of the properties of PSD matrices is that all their eigenvalues are real and positive. In fact, some SPICE simulators check for this condition before simulating circuits having coupling coefficients k defined among its inductors (using component K).

If the measured inductance matrix is not PSD, then the measuring procedure has to be analyzed and corrected, to assure that the resulting matrix is PSD. Experimentation shows that, besides the windings' number (matrix dimension), coupling and turns' ratio between windings strongly influence correct measurement results (that yield to a PSD matrix).

Approaching the problem from a more physical point of view has been done in [12]–[15]. These references propose similar measurement methods based on energy balance and Maxwell equations and comparing them to a finite-elements model (FEM) in order to measure the self, mutual, and leakage inductance. Mathematical complexity of energy balance and Maxwell equations make this approach unpractical for more than three windings.

The following general methods have been identified in the technical literature.

1) Short-open (SO) method.
2) Differential-cumulative (DiC) method.
3) Cross-voltage-to-current (xVI) method

The classical method to measure the leakage and magnetizing inductance directly is the SO circuit technique, where one winding is shorted to measure the leakage inductance and afterward left open to measure the magnetizing inductance. But, this technique is not very useful for an MCI.

In [20], the DiC method is presented and it is demonstrated that this method improves the results obtained with the described short- and open-circuit method. The DiC method is directly applicable to measure a complex inductance matrix.

Another characterization method described in [6], [7], and [21] (called by the authors xVI), proposes to measure the voltage-to-current ratio across different windings. But, the xVI method has been discarded for two reasons. First, the difficulty of measuring high frequency, low amplitude signals and, second, the distortion of the sinusoidal signals, that makes it very difficult to compare input and output amplitudes. Large turns' ratio and low inductances, make these two reasons even more important. This results in a high error in the measurement and, therefore, in the calculated mutual inductances.

Applying the different methods found in the technical literature to MCI with different turns' ratio or large coupling coefficients between them, could lead to a result where the inductance matrix is non-PSD, and even worse, a coupling coefficient matrix with some of its elements larger than one, ($k_{ij} > 1$). There are several causes for this result, either the measuring equipment is not precise enough, the methods are not appropriate due to some of the problems mentioned above or due to the loss of accuracy.

Therefore, the authors propose a new method to characterize MCI, whose resulting inductance matrix is PSD.

C. Definition of Concepts

Basic concepts are reviewed in this section to help the reader to understand the paper. The inductance matrix is defined as

$$\mathbf{L} = \begin{pmatrix} L_{11} & L_{12} & \dots & L_{1n} \\ L_{21} & L_{22} & \dots & L_{2n} \\ \vdots & \vdots & \ddots & \vdots \\ L_{n1} & L_{n2} & \dots & L_{nn} \end{pmatrix} \tag{1}$$

where L_{ii} are the self inductances and L_{ij} are the mutual inductances.

The coupling coefficients matrix represents the coupling coefficient of each winding to each other [17].

The elements of the coupling coefficient matrix related to two different windings, L_{ii} and L_{jj}, are given by

$$k_{ij} = \frac{L_{ij}}{\sqrt{L_{ii} L_{jj}}}. \tag{2}$$

The inductance matrix can be related to the coupling coefficient matrix with the following matrix product:

$$\mathbf{L} = \mathbf{D} \cdot \mathbf{k} \cdot \mathbf{D} \tag{3}$$

where $\mathbf{D}$ is a diagonal matrix defined by

$$D_{ij} = \begin{cases} \sqrt{L_{ii}}, & \text{if } i = j \\ 0, & \text{if } i \neq j. \end{cases} \tag{4}$$

Therefore, the coupling matrix can be considered the normalized inductance matrix. In addition, the coupling matrix is PSD, if and only if the inductance matrix is PSD.

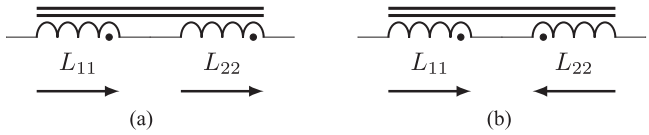

Fig. 1. Windings' connection to measure the mutual inductance between two windings, L_{11} and L_{22}, applying the DiC method. (a) Cumulative measurement $L_{\mathrm{s}\,12}$. (b) Differential measurement $L_{\mathrm{o}\,12}$.

II. Differential-Cumulative Method

The DiC method, described in [20], is the most accurate measuring technique for an MCI known so far. The DiC method is used to characterize coupled inductors and to do so it groups the windings in pairs and measures the total inductance of its two configurations, in phase and in opposing phase. To properly apply the method, we need to know the dot (phasing or winding sense) of each winding, as shown in Fig. 1.

The mutual inductance (L_{ij}) is calculated applying (5)

$$L_{ij} = \frac{L_{\mathrm{s}\,ij} - L_{\mathrm{o}\,ij}}{4} \tag{5}$$

and its related coupling coefficient is

$$k_{ij} = \frac{L_{\mathrm{s}\,ij} - L_{\mathrm{o}\,ij}}{4\sqrt{L_{ii}L_{jj}}}. \tag{6}$$

The self inductances, L_{ii} and L_{jj}, are measured directly on each winding.

Practical measurements show that the resulting matrix when using this measurement method is not always PSD, which suggests that its application is limited to certain conditions.

A. Accuracy of the DiC Method

The relative error of the results obtained with the DiC method has been calculated to analyze its limitations.

The relative error of the mutual inductance, $\varepsilon L_{ij}/L_{ij}$, with this method is given by

$$\frac{\varepsilon L_{ij}}{L_{ij}} = \frac{L_{\mathrm{s}\,ij}}{L_{\mathrm{s}\,ij} - L_{\mathrm{o}\,ij}}\frac{\varepsilon L_{\mathrm{s}\,ij}}{L_{\mathrm{s}\,ij}} + \frac{L_{\mathrm{o}\,ij}}{L_{\mathrm{s}\,ij} - L_{\mathrm{o}\,ij}}\frac{\varepsilon L_{\mathrm{o}\,ij}}{L_{\mathrm{o}\,ij}}. \tag{7}$$

The relative error of the coupling coefficient, $\varepsilon k_{ij}/k_{ij}$, is given by

$$\frac{\varepsilon k_{ij}}{k_{ij}} = \frac{\varepsilon L_{ij}}{L_{ij}} + \frac{1}{2}\frac{\varepsilon L_{ii}}{L_{ii}} + \frac{1}{2}\frac{\varepsilon L_{jj}}{L_{jj}}. \tag{8}$$

Both (7) and (8) clearly show that the relative error of the L_{ij} and k_{ij} will increase rapidly for similar values of $L_{\mathrm{s}\,ij}$ and $L_{\mathrm{o}\,ij}$. To perform a simplified analysis, we will suppose that the relative error of all inductance measurements is the same and equal to $\varepsilon L/L$. This is only a rough approximation but allows to have a better insight into these equations

$$\frac{\varepsilon L}{L} \approx \frac{\varepsilon L_{\mathrm{s}\,ij}}{L_{\mathrm{s}\,ij}} \approx \frac{\varepsilon L_{\mathrm{o}\,ij}}{L_{\mathrm{o}\,ij}} \approx \frac{\varepsilon L_{ii}}{L_{ii}} \approx \frac{\varepsilon L_{jj}}{L_{jj}}. \tag{9}$$

This converts (7) for the mutual inductance into

$$\frac{\varepsilon L_{ij}}{L_{ij}} = \frac{L_{\mathrm{s}\,ij} + L_{\mathrm{o}\,ij}}{L_{\mathrm{s}\,ij} - L_{\mathrm{o}\,ij}}\frac{\varepsilon L}{L}. \tag{10}$$

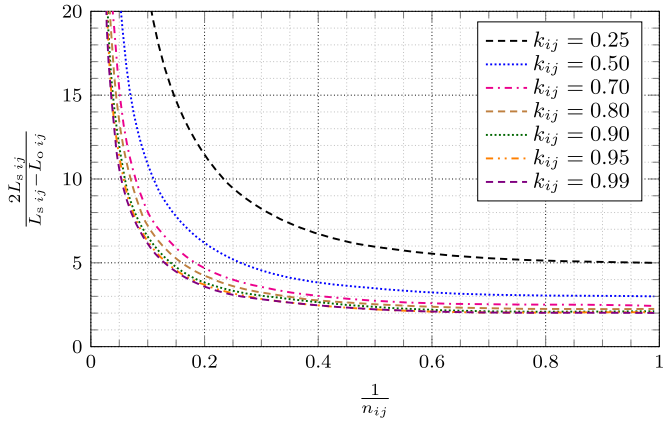

Fig. 2. Factor $\frac{2L_{\mathrm{s}\,ij}}{L_{\mathrm{s}\,ij}-L_{\mathrm{o}\,ij}}$, affecting the relative error of k_{ij} [see (13) found in (11)], as a function of $\frac{1}{n_{ij}}$ and k_{ij} for the DiC method.

It also converts (8) for the coupling coefficient into

$$\frac{\varepsilon k_{ij}}{k_{ij}} = \frac{2L_{\mathrm{s}\,ij}}{L_{\mathrm{s}\,ij} - L_{\mathrm{o}\,ij}}\frac{\varepsilon L}{L}. \tag{11}$$

The two factors that multiply the relative error $\varepsilon L/L$ in (10) and (11), are of importance. Only the case of (11) is going to be studied here, but the results also apply to (10).

If we take into account the influence of the turns' ratio $n_{ij} = \sqrt{L_{ii}/L_{jj}}$ and coupling coefficient k_{ij} in $L_{\mathrm{s}\,ij}$ and $L_{\mathrm{o}\,ij}$ and normalize them with respect to L_{ii}, we will be able to analyze how n_{ij} and k_{ij} affect the relative error of the DiC method. Based on Fig. 1 it is easy to calculate the expression shown as

$$\frac{L_{\mathrm{s/o}\,ij}}{L_{ii}} = 1 + \frac{1}{n_{ij}^2} \pm 2\frac{k_{ij}}{n_{ij}}. \tag{12}$$

Inserting (12) into the factor of (11), we obtain the following expression:

$$\frac{2L_{\mathrm{s}\,ij}}{L_{\mathrm{s}\,ij} - L_{\mathrm{o}\,ij}} = \frac{1 + \frac{1}{n_{ij}^2} + 2\frac{k_{ij}}{n_{ij}}}{2\frac{k_{ij}}{n_{ij}}}. \tag{13}$$

If we represent (13) graphically we will easily appreciate the influence of n_{ij} and k_{ij} in the relative error.

Fig. 2 clearly shows that the relative error factor shown in (13) increases very fast when $\frac{1}{n_{ij}} < 0.2$ for any k_{ij}. In fact the factor becomes larger for smaller k_{ij}. This means that for very different turns' number between L_{ii} and L_{jj}, the DiC method will lose accuracy very fast.

On the other hand, the authors have detected experimentally that the DiC method also provides larger values of k_{ij} as expected when $\frac{1}{n_{ij}} = 1$ and $k_{ij} > 0.9$. The measured values are usually too close to one (0.999 or even 1.000) or even greater than one. But, this error observed is not due to the relative error factor, as shown in Fig. 2. Two other reasons are given, both mechanical and physical that could lead to this error.

Therefore, three reason, related to specific conditions, have been identified where the DiC method is not accurate enough and could lead to wrong measurements.

1) When $L_{ii} \gg L_{jj}$, which means $1/n_{ij} \ll 1$ (for any k_{ij}), then $L_{\mathrm{s}\,ij} \approx L_{\mathrm{o}\,ij}$ and the relative error of k_{ij} and L_{ij} increases rapidly. In other words, for a very small (or large) turns' ratio of two windings, if the DiC method is used to measure the coupling coefficient, the result will have a very large relative error.
2) When $1/n_{ij} = 1$ and $k_{ij} \approx 1$, then both windings have been wound in parallel and very tightly around the core. So, the phasing dots of both windings will be close together. Considering Fig. 1, it can be deduced that the differential measurement will need a very short wire connection compared to the cumulative measurement. Even choosing the long wire to measure both configurations and trying to keep the area spanned by this wire the same, the measurement of $L_{\mathrm{s}\,ij}$ will tend to be greater and $L_{\mathrm{o}\,ij}$ smaller. This means that the resulting k_{ij} [see (6)] and its equivalent L_{ij} [see (5)] will be larger as well.
3) Finally, the flux density found in the core under configuration (a) [flux of both inductors is added] is different from configuration (b) [flux of both inductors is canceled out] of Fig. 1. If the dependence of the relative permeability with the flux density [22] is considered, then $L_{\mathrm{s}\,ij}$ will be as it should be but $L_{\mathrm{o}\,ij}$ will be smaller than it should be. Again, this means that the resulting k_{ij} [see (6)] and its equivalent L_{ij} [see (5)] will be larger. This effect is material dependent and manufacturers usually provide permeability changes for fluxes above $1\,mT$.

The first reason is important enough not to be neglected and the other two will have a small effect but add together and appear when very critical measurements have to be done. Having identified these problems, this paper proposes a new method that should be used for MCI with large values of k_{ij} or coupled inductor pairs with dissimilar turns' number to measure correct and accurate PSD inductance matrices.

III. Resonance Method

The new characterization method proposed in this paper has been called the resonance (RE) method. The aim of the RE method is to measure both the self and mutual inductance (resulting in a PSD inductance matrix) using an external resonance capacitor C_r by analyzing the MCI in the frequency domain. The method should at least provide a correct measurement (a PSD inductance matrix) where the DiC method fails (dissimilar turns' number or tightly coupled inductors).

Having the setup shown in Fig. 3, where C_r is loading winding L_{22} and all other windings are left open, the absolute value of the impedance $|Z|$ seen into winding L_{11} can be studied.

Once the resonance frequencies of $|Z|$ are measured, the self and mutual inductances can be calculated, as will be demonstrated later. The self and mutual inductance for other windings are measured changing the capacitive load, C_r to another winding (L_{11}, L_{22},..., L_{nn}) and measuring the impedance seen at each other of the different windings.

A. Impedance Study

The study of impedance $|Z|$ includes the parasitic resistance, as shown in Fig. 3. Frequency dependence of core losses, skin effect, and proximity effect are not all included in the series resistances, but can be represented with mutual resistances, as shown in [23] and [24]. The influence of the shown resistances and mutual resistances will be studied later on. Losses represented by mutual resistances will be neglected if their value is of the same order or smaller than the diagonal elements of the resistance matrix. As shown later, its influence in the measurement is not altering the results.

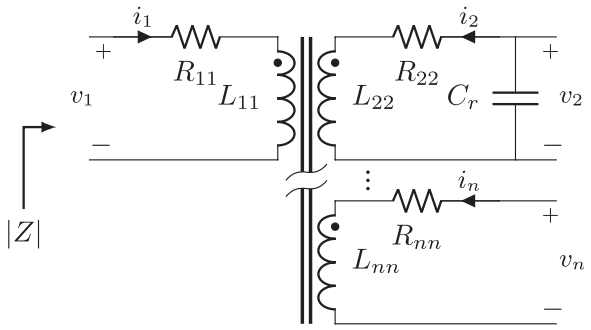

Fig. 3. Application of the RE method. $|Z|$ is measured loading one secondary winding with C_r.

The equations system of the circuit shown in Fig. 3, where v_i is the winding voltage, i_i is the winding current, and s is the Laplace variable, can be expressed in matrix form as follows:

$$\begin{pmatrix} v_1 \\ v_2 \\ \vdots \\ v_n \end{pmatrix} = \left[\begin{pmatrix} L_{11} & L_{12} & \dots & L_{1n} \\ L_{21} & L_{22} & \dots & L_{2n} \\ \vdots & \vdots & \ddots & \vdots \\ L_{n1} & L_{n2} & \dots & L_{nn} \end{pmatrix} \cdot s + \begin{pmatrix} R_{11} & R_{12} & \dots & R_{1n} \\ R_{21} & R_{22} & \dots & R_{2n} \\ \vdots & \vdots & \ddots & \vdots \\ R_{n1} & R_{n2} & \dots & R_{nn} \end{pmatrix} \right] \cdot \begin{pmatrix} i_1 \\ i_2 \\ \vdots \\ i_n \end{pmatrix}. \quad (14)$$

As seen in Fig. 3, all but winding L_{22} are in open circuit, and therefore, their currents are zero (i_3 to i_n are zero).

We are only interested in the winding pair L_{11} and L_{22} and, so, we only take into account the expressions of v_1 and v_2 of (14).

The capacitive load is connected to winding L_{22} (see Fig. 3) and then the voltage between its terminals is

$$v_2 = -\frac{1}{C_r\, s}\, i_2. \quad (15)$$

$Z = v_1/i_1$ can be derived, if (15) is replaced into the expression of v_2 of (14), then finding an expression for i_2 and replacing it into the expression of v_1 of (14). Taking into account that $L_{12} = L_{21}$, the total impedance seen into winding L_{11} is

$$Z(s) = \frac{v_1}{i_1} = R_{11} + L_{11}s - \frac{C_r s(L_{12}s + R_{12})^2}{1 + C_r R_{22} s + C_r L_{22} s^2}. \quad (16)$$

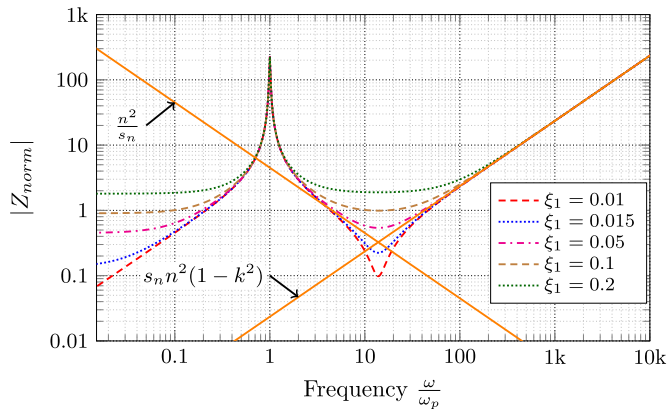

Fig. 4. Bode plot of $|Z_{\text{norm}}|$ for several values of parameter ξ_1 and keeping $\xi_2 = 0$ ($k = 0.997$, $n = 2.123$).

B. Analysis of the Ideal Impedance Expression

If we neglect the resistances (hence $R_{11} = R_{22} = R_{12} = 0$), we can simplify (16) and obtain the expression of the ideal impedance

$$Z_{\text{ideal}}(s) = \frac{L_{11}s + C_r(L_{11}L_{22} - L_{12}^2)s^3}{1 + C_r L_{22} s^2}. \tag{17}$$

We can easily calculate zeros and poles and their corresponding resonance frequencies. The resonance frequency of the pole ω_p is given by (18) and the resonance frequency of the zero ω_z is given by (19)

$$\omega_p = \frac{1}{\sqrt{L_{22}C_r}} \tag{18}$$

$$\omega_z = \frac{1}{\sqrt{L_{22}C_r}} \frac{1}{\sqrt{1 - \frac{L_{12}^2}{L_{11}L_{22}}}} = \frac{\omega_p}{\sqrt{1 - \frac{L_{12}^2}{L_{11}L_{22}}}}. \tag{19}$$

Combining both ω_p and ω_z with (2), an expression for k_{12} can be derived.

$$k_{12} = \sqrt{1 - \frac{\omega_p^2}{\omega_z^2}}. \tag{20}$$

Graphically, this means that looking at the Bode plot of the impedance (see Fig. 4), the "distance" in frequency between both resonance frequencies is related to the coupling coefficient. The larger the "distance" between resonance frequencies is, the larger the coupling coefficient is.

Otherwise, and based on the first part of (19), the mutual inductance L_{12} can be calculated using the following expression:

$$L_{12} = \sqrt{L_{11}L_{22} - \frac{L_{11}}{C_r\omega_z^2}}. \tag{21}$$

Taking two windings at each time and repeating this process for any two pair of windings, allows us to calculate all mutual inductances.

C. Accuracy of the RE Method

The RE method accuracy will be calculated in order to compare to the previously calculated accuracy of the DiC method. The relative error of k_{ij} with this method [based on (20)] is given by

$$\frac{\varepsilon k_{ij}}{k_{ij}} = \frac{\omega_p^2}{\omega_z^2 - \omega_p^2}\left(\frac{\varepsilon\omega_p}{\omega_p} + \frac{\varepsilon\omega_z}{\omega_z}\right). \tag{22}$$

Using (20), we can rewrite (22) into

$$\frac{\varepsilon k_{ij}}{k_{ij}} = 2\frac{1 - k_{ij}^2}{k_{ij}^2}\frac{\varepsilon f}{f} \tag{23}$$

where the relative error of f_p and f_z, which is the same as the relative error of ω_p and ω_z, has been supposed to be the same and equal to $\varepsilon f/f$. Equation (23) clearly shows that the relative error becomes small when $k_{ij} \approx 1$, but large for $k_{ij} \ll 1$. L_{ij} will be calculated knowing k_{ij} and using (2), and its accuracy will depend on the accuracy of k_{ij}. The turns' ratio n_{ij} has no influence on (23).

The influence of other parameters are studied, hereafter, to know the limitations of the RE method.

D. Normalization of the Impedance Expression

To perform a more generalized analysis of the impedance expressions and the method itself, normalized expressions are going to be derived.

First, we normalize the ideal impedance represented by (17).

The impedance has been normalized to the characteristic impedance of the resonant tank Z_r and the frequency has been normalized to the resonance frequency of the pole ω_p. The new normalized impedance is, therefore, defined as

$$Z_{\text{ideal\_norm}}(s_n) = \frac{Z_{\text{ideal}}(s)}{Z_r} \text{ where } Z_r = \sqrt{\frac{L_{22}}{C_r}},\ s_n = \frac{s}{\omega_p} \tag{24}$$

and (17) now becomes

$$Z_{\text{ideal\_norm}}(s_n) = n^2\left(s_n\frac{\left(1 - k_{12}^2\right)s_n^2 + 1}{s_n^2 + 1}\right) \tag{25}$$

where n is the turns' ratio and defined as

$$n = \sqrt{\frac{L_{11}}{L_{22}}}. \tag{26}$$

Using (24) and (26) and defining the damping factors ξ_1, ξ_2, and ξ_{12} as

$$\xi_1 = \frac{R_{11}}{2L_{11}\omega_p}, \quad \xi_2 = \frac{R_{22}}{2L_{22}\omega_p}, \quad \xi_{12} = \frac{R_{12}}{2L_{11}\omega_p} \tag{27}$$

the real impedance expression (16) can be normalized as well

$$Z_{\text{norm}}(s_n) = n^2\left(2\xi_1 + s_n - s_n\frac{(k_{12}s_n + n2\xi_{12})^2}{s_n^2 + 2\xi_2 s_n + 1}\right). \tag{28}$$

E. Influence of the Winding Resistance

In this section, the influence of the resistances R_{11}, R_{22}, and R_{12} on the expression of the impedance shown in (16) is

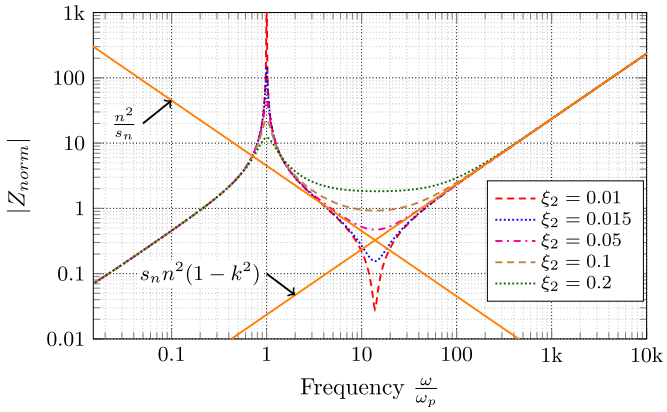

Fig. 5. Bode plot of $|Z_{\text{norm}}|$ for several values of parameter ξ_2 and keeping $\xi_1 = 0$ ($k = 0.997$, $n = 2.123$).

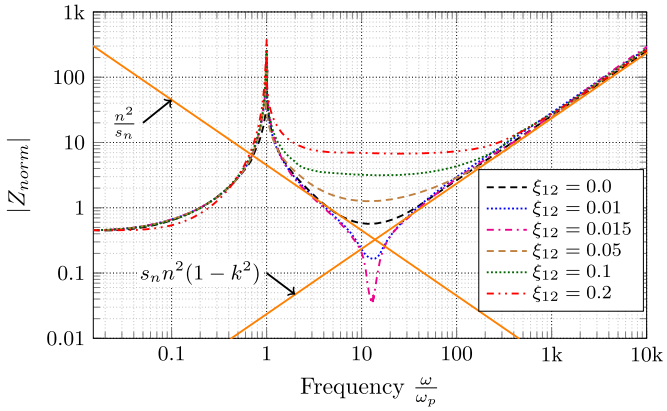

Fig. 6. Bode plot of $|Z_{\text{norm}}|$ for several values of parameter ξ_{12} and keeping $\xi_1 = 0.05$ and $\xi_2 = 0.01$ ($k = 0.997$, $n = 2.123$). It can be observed that some values of ξ_{12} partially cancel the damping effect of ξ_1 and ξ_2.

presented. This influence has to be known to evaluate the valid range of applicability of the RE characterization method.

In order to perform a generalized study we will analyze $|Z_{\text{norm}}|$ represented by (28) in relation to ξ_1, ξ_2, and ξ_{12}.

Fig. 4 shows the influence of ξ_1 in the normalized impedance $|Z_{\text{norm}}|$ for a given coupling coefficient k [called k_{12} in (28)] and a turns' ratio n. It can be seen that ξ_1 only affects the second resonance, which corresponds to the zero of the impedance. The second resonance can degenerate fading out the effect of the zero (see Fig. 4) for large values of ξ_1.

Due to the fact, that the RE method relies on precisely reading the resonance frequencies, it is clear that a higher accuracy is achieved when the resonance is less damped.

Fig. 5 shows the influence of ξ_2 in the normalized impedance $|Z_{\text{norm}}|$. In this case, the variation of the ξ_2 affects both resonance frequencies, the zero and the pole.

Fig. 6 shows clearly that ξ_{12} only affects the zero of the impedance. The most interesting behavior is that its effect is not monotone growing because some values of ξ_{12} (for example $\xi_{12} = 0.015$) damp less than smaller values ($\xi_{12} = 0$). But, this behavior is of little help as it cannot easily be predicted. Thus, the limit for ξ_1 and ξ_2 that degrades $|Z_{\text{norm}}|$ can be considered the worst case, because the influence of ξ_{12} is smaller. Therefore, the rest of the analysis will be focused only on ξ_1 and ξ_2 neglecting ξ_{12}. In any case, if the resonance frequencies become degraded by any factor, it is clear that the RE method could not be used.

The next sections show which values of ξ_1 and ξ_2 limit the use of the proposed RE method.

1) Maximum Value for ξ_2: It is important to know the maximum acceptable value for ξ_2 before the RE method becomes useless. It is assumed that the impedance does not provide useful information of its zeros and poles when they degenerate (and so does the expression of the impedance). $|Z_{\text{norm}}|$ degenerates when the imaginary part of the pole is equal to zero. The expression of the poles of $|Z_{\text{norm}}(s_n)|$, presented in (29), has to be analyzed

$$s_{n,p} = -\xi_2 \pm \sqrt{\xi_2^2 - 1}. \tag{29}$$

As the imaginary part is given by the square root [see (29)], the pole degenerates if the radicand becomes equal or greater than zero.

Therefore, the only acceptable values for ξ_2 have to fulfill the following condition:

$$\xi_2 < 1. \tag{30}$$

Equation (30) corresponds in the circuit (see Fig. 3) to the following equation:

$$R_{22} < 2\sqrt{\frac{L_{22}}{C_r}}. \tag{31}$$

If the pole of $|Z_{\text{norm}}|$ fulfills (30), the pole will not degenerate. This statement applies also to (31). Note that (31) depends on the resonant capacitor C_r. Then, if the capacitor has a high value, the maximum value of R_{22} will decrease and the pole will degrade faster.

2) Maximum Value for ξ_1: In this case, the degeneration of the zero cannot be directly related to the condition of having the imaginary part of the zeros equal to zero, as the expression of the numerator of (28) is a third-order equation. Therefore, two different conditions have been applied to find out when the zero degenerates and its frequency becomes difficult to read.

The two conditions are as follows.

1) It is considered that the zero frequency is degenerated and it can be hardly read from the Bode plot (see Fig. 5, for example for $\xi_2 = 0.1$, where the local minimum of $|Z_{\text{norm}}|$ is not so clear anymore), when the amplitude of the crossing point of the two asymptotes [n^2/s_n and $s_n\, n^2(1-k^2)$] at each side of the frequency of the zero of $|Z_{\text{norm}}|$ is less than the amplitude of $|Z_{\text{norm}}|$ itself at this frequency. In Fig. 5, this condition applies when $\xi_2 > 0.05$.
2) It is considered that the natural frequency of the zero is different to the frequency of the local minimum of the Bode plot. This difference becomes larger the higher the damping factor ξ_2 is. This condition is more restrictive than the previous one.

The graphical solution of the first condition is shown in Fig. 7.

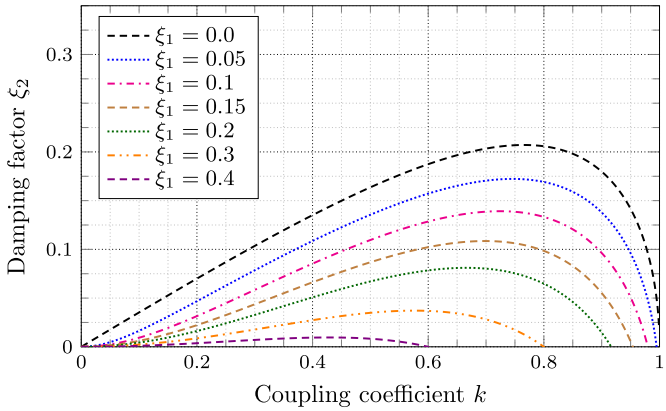

Fig. 7. Graph that represents for which values of ξ_2 related to k, the amplitude of $|Z_{\text{norm}}|$ becomes smaller than the amplitude of the crossing point of the asymptotes at both sides of the series resonance of $|Z_{\text{norm}}|$, and thus, having a degenerated zero. ξ_1 is swept as parameter.

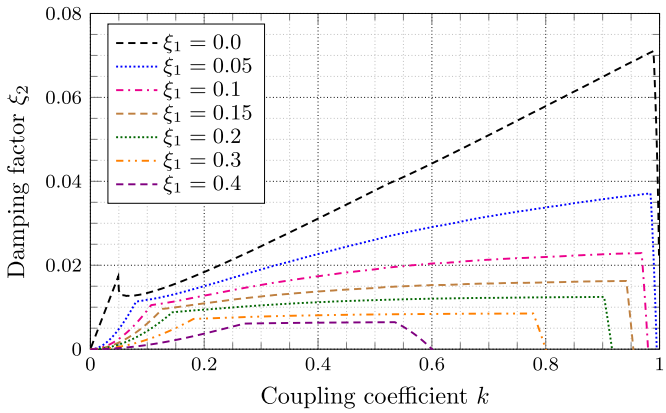

Fig. 8. Graph that combines condition of the error introduced by the difference between the natural frequency and the minimum (zero) frequency of the Bode plot (limit established at 1%) and Fig. 7. This graph represents for which values of ξ_2 related to k, the zero of $|Z_{\text{norm}}|$ degenerates. ξ_1 is swept as parameter.

When applying the second more restrictive condition to Fig. 7, Fig. 8 is obtained, which gives even smaller values for ξ_2 as critical condition to read the zero frequency.

From Fig. 8, it can be concluded that, as expected, ξ_1 and ξ_2 limit the readability of the zero of $|Z_{\text{norm}}|$, which is needed to determine the coupling coefficient and the mutual inductance with the proposed method. Fig. 8 also shows a maximum for different values of k and this maximum depends on ξ_1 and ξ_2. For low coupling coefficients k, the influence of ξ_1 and ξ_2 becomes critical and the proposed method could become useless. For large coupling coefficients k, the influence of ξ_1 and ξ_2 becomes less critical and it usually corresponds to unrealistic values. Thus it can be concluded that the proposed method is appropriate for large values of coupling coefficient, k. As normalized values have been used during all the study, they can be denormalized for any real application.

3) Frequency Deviation of Pole and Zero: As already mentioned before, the difference between natural frequency and the local maximum and minimum of the impedance plays an important role. The proposed method relies on the readout of the

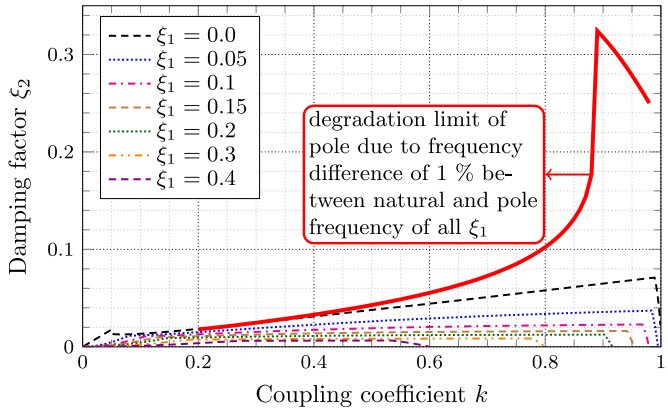

Fig. 9. Graph that combines Fig. 8 and the error introduced by the difference between the natural frequency and the maximum (pole) frequency of the Bode plot (limit established at 1%). This graph represents for which values of ξ_2 related to k, the zero and the pole of $|Z_{\text{norm}}|$ degenerate. ξ_1 is swept as parameter.

local maximum and minimum frequency of the Bode plot of the impedance, but if the read out frequency does not correspond to the natural frequency, then the calculation of the coupling coefficient k will not be correct. The authors have, thus, performed an analysis checking for an error of less than $1\,\%$ between both frequencies, local maximum or minimum, and the corresponding natural frequency.

Part of this study was already done in Section III-E2 for the zero, but the analysis for the pole has not yet been shown. A first limit obtained for the pole is expressed by (30), but it has still to be checked if the ratio between the pole and maximum frequency is less than $1\,\%$. This last condition has been added to Fig. 8, and is shown in Fig. 9.

Fig. 9 clearly shows that the conditions found for the zero are more restrictive than the condition for the pole. Thus, once the conditions for the zero (see Fig. 8) are fulfilled, then the read out of the pole has an error much smaller than $1\,\%$.

F. Capacitor Selection

Another very important point for a correct result when applying the RE method is to choose the right resonance capacitor C_r. This strongly depends on the parasitic capacitance present in the magnetic element and related to the two windings under measurement.

In order to measure the overall parasitic capacitance, the capacitive slope of the impedance Bode plot, without an external resonance capacitor can be used. This slope corresponds to the slope of the line connecting the pole and the zero. As an example, Fig. 10 shows a measured Bode plot of a three-phase transformer having all its windings in the open circuit, where the capacitive behavior and the line mentioned earlier is shown and labeled by "C."

It is clear that the load capacitor C_r must be much greater than the parasitic capacitance, because when the capacitor is connected to the secondary winding, the total impedance $|Z|$ reflected to the primary, sums all the capacitors of the magnetic element $C_{\text{total}} = C_r + \sum_{k=0}^{i} C_{p_k}$. Therefore, the load

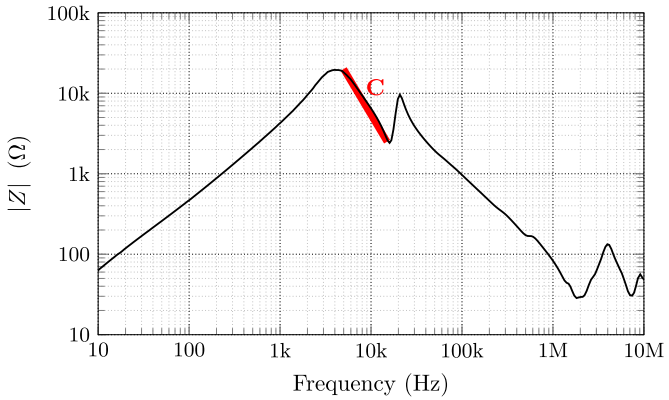

Fig. 10. Measured impedance, $|Z|$, of a three-phase transformer with all secondaries in the open circuit. The thick line, called "C," highlights the capacitive behavior.

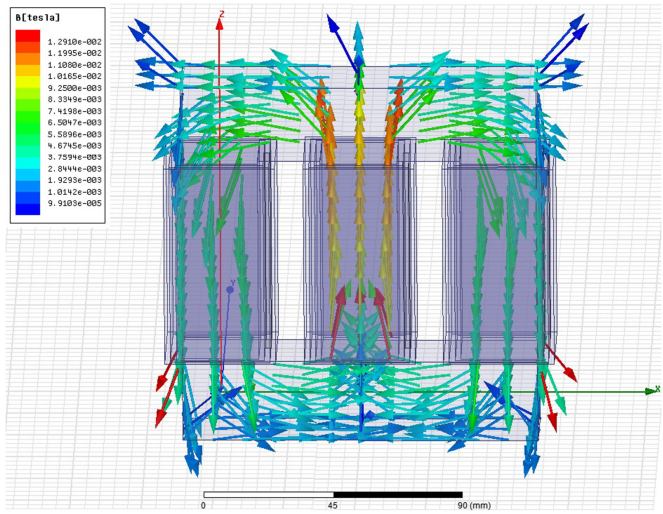

Fig. 11. Physical model of the three-phase inductor used by Maxwell 3D to perform an FEA. The eddy currents method was used, supposing $\mu_r = 800$, a gap of 0.25 mm, at a frequency of 50 Hz.

capacitor C_r should be ten to hundred times larger than the overall parasitic capacitors ($C_r \gg C_{\text{total parasitics}}$). Then, the parasitic capacitance can be neglected and will not affect the measurement.

But, an excessive value of the resonance capacitor C_r influences the degradation of $|Z_{\text{norm}}|$, because C_r appears in (18) and ω_p appears in ξ_1 and ξ_2 [see (27)]. This could be written as having C_r within the following range:

$$C_{\text{total parasitics}} \ll C_r < \min\left(4\xi_1^2 n^2 \frac{L_{11}}{R_{11}^2},\ 4\xi_2^2 \frac{L_{22}}{R_{22}^2}\right) \qquad (32)$$

Based on the limit shown in Fig. 8, for $k = 0.9$, the limits chosen could be $\xi_1 = 0.1$ and $\xi_2 = 0.02$, which allows us to calculate the extreme values of the range of C_r with (32).

G. Applicability

Having studied the influence of parasitics in the proposed RE method, two statements can be done regarding the applicability of the RE method.

1) The parasitic elements have a stronger influence at low values of the coupling coefficient, k (see Fig. 8).
2) The RE method works best for large values of coupling coefficient k because the resonances are farther away from each other in the frequency domain [see (20)]. For low values of k both frequencies become close together and it will be much more difficult to measure them, because both magnitudes of the impedance will be similar and high frequency resolution will be necessary.

These statements add up to the accuracy already discussed in Section III-C.

IV. Finite-Element Analysis (FEA)

Once the new RE method has been analyzed and the already known DiC method has been explained, the authors suggest to make an FEA in order to crosscheck a measured coupling coefficient matrix. The FEA provides the user with a simulated physical approach of the coupling coefficient matrix and helps to identify which calculated values can be right and which can be wrong.

If both methodologies (RE and DiC) are applied to measure, for example, a three-phase inductor, both can result in PSD matrices but having different elements. The question that arises is which of the both matrices is correct. Using the simulated coupling coefficient matrix obtained with the FEA, the user can know which of the measurements is closer to the simulation, and therefore, identify which one is the more accurate one.

Fig. 11 shows a simplified structure of a three-phase inductor that will be used to run the FEA and to demonstrate which of the measured coupling coefficients are correct.

The resulting coupling coefficient matrix is equal to

$$k_{12} = 0.511 \quad k_{13} = 0.295 \quad k_{23} = 0.494. \qquad (33)$$

These values allow us to know what are the expected measured values for these coupling coefficients and select the correct matrix in case we have measured two PSD matrices with two methods and have reached two different results.

V. Experimental Validation

In this section, three different coupled inductors are characterized with the two methods already explained, namely DiC and RE. The results of both methods are compared with each other and the resulting matrices have been checked for the PSD condition. These experiments will demonstrate the applicability of both methods related to the coupling coefficient k.

The measurement equipment has been LCR meter 4284A (for DiC) and network analyzer E5061B (for RE), both from Agilent and calibrated and compensated.

The three coupled inductors are measured, listed, hereafter, have different cores, and correspond to different applications.

1) Coupled inductor with five windings on an iron powder toroidal core with different coupling coefficients and turns' ratio to test all possible conditions studied.

Fig. 12. Five windings' coupled inductor on an iron powder core. On the left side are three well coupled windings and on the right side two well coupled windings. But these last two windings are not so well coupled to the first three ones.

2) Output filter coupled inductor with seven windings on a molypermalloy powder (MPP) toroidal core where all its coupling coefficients are close to one.
3) Three-phase grid filter inductor with three windings wound on three laminated-iron core legs. Coupling coefficients are expected to be small.

A. *Five Windings on Iron Powder Toroid*

The first magnetic element consists on a toroidal core (Micrometals T130-26) with five windings. Three windings of twenty, twenty, and five turns have been wound very tightly coupled on one side and two windings of twenty and five turns have also been wound tightly coupled on the other side (see Fig. 12). The turns' ratio and the coupling coefficients between the different windings, therefore, change from one to the other. The inductor has been soldered to a PCB and pins have been placed on the back to avoid any movement of the windings which could alter the measured inductance.

Both methods (DiC and RE) have been applied to measure the inductance matrix of this coupled inductor. The capacitor used for the RE method is $C_r = 1\ \mu$F, having a lower limit of $C_{r\,\min} = 142$ pF and an upper limit of $C_{r\,\max} = 10.9\ \mu$F (see (32)). The frequency chosen for the DiC method was 100 kHz.

The used core covers all possible cases: $n = 1$, $n \ll 1$, $k \approx 1$ and $k < 1$. The turns' ratio is shown, hereafter, [see (34)] and the approximate factors multiplying the relative error [called error factor as seen in (35) and (36)] have also been calculated [based on (13) and (23)]. The relative error has not been calculated at this time because it depends on the relative error of the measurement instrument, which in our case are very different and does not allow us to fairly compare both results (for 4284 A, $0.08\% < \varepsilon L/L < 16.94\%$, and for E5061B, $\varepsilon f/f \approx 0.000007\%$). The approximate error factors given provide a better insight comparing the accuracy of both methods independently of the measurement instrument. Measurement instrument clearly plays a crucial role in accuracy, but when comparing both methods the results could be misleading. In this case only the RE coupling coefficient matrix is PSD.

$$n = \begin{pmatrix} 1 & 1.00 & 0.25 & 1.00 & 0.25 \\ 1.00 & 1 & 0.25 & 1.00 & 0.25 \\ 0.25 & 0.25 & 1 & 0.25 & 1.00 \\ 1.00 & 1.00 & 0.25 & 1 & 0.25 \\ 0.25 & 0.25 & 1.00 & 0.25 & 1 \end{pmatrix} \tag{34}$$

$$k_{\text{DiC}} = \begin{pmatrix} 1 & 1.000 & 0.943 & 0.710 & 0.668 \\ 1.000 & 1 & 0.941 & 0.709 & 0.667 \\ 0.943 & 0.941 & 1 & 0.625 & 0.584 \\ 0.710 & 0.709 & 0.625 & 1 & 0.970 \\ 0.668 & 0.667 & 0.584 & 0.970 & 1 \end{pmatrix}$$

$$\text{and error factor of } k_{\text{DiC}} = \begin{pmatrix} & 1.01 & 2.18 & 1.42 & 3.03 \\ 1.01 & & 2.18 & 1.42 & 3.04 \\ 2.18 & 2.18 & & 3.30 & 1.75 \\ 1.42 & 1.41 & 3.30 & & 2.10 \\ 3.03 & 3.04 & 1.75 & 2.10 & \end{pmatrix} \tag{35}$$

$$k_{\text{RE}} = \begin{pmatrix} 1 & 0.994 & 0.915 & 0.702 & 0.646 \\ 0.994 & 1 & 0.913 & 0.705 & 0.658 \\ 0.915 & 0.913 & 1 & 0.615 & 0.584 \\ 0.702 & 0.705 & 0.615 & 1 & 0.950 \\ 0.646 & 0.658 & 0.584 & 0.950 & 1 \end{pmatrix}$$

$$\text{and error factor of } k_{\text{RE}} = \begin{pmatrix} & 0.02 & 0.39 & 2.06 & 2.79 \\ 0.02 & & 0.40 & 2.02 & 2.62 \\ 0.39 & 0.40 & & 3.30 & 3.87 \\ 2.06 & 2.02 & 3.30 & & 0.22 \\ 2.79 & 2.62 & 3.87 & 0.22 & \end{pmatrix}. \tag{36}$$

The error factors of this experiment confirm the hypothesis that magnetic elements with very different turns' ratio will be more error prone than with $n = 1$ with the DiC method.

The other two reasons affecting the accuracy of the DiC method and explained in Section II can be detected in (35), where the coupling coefficient of the two windings having 20 tightly coupled turns ($n = 1$) is measured to be 1.000. The authors think that this value is not real and the correct value will be closer to the measurement of the RE method, which is 0.994. Not only the values are better measured with the RE method but also its error factor is much smaller. Thus, larger coupling coefficients k are also better measured with the RE method.

In addition and to check how the frequency affects the RE method, all the coupling coefficients have been measured with several resonant capacitors C_r.

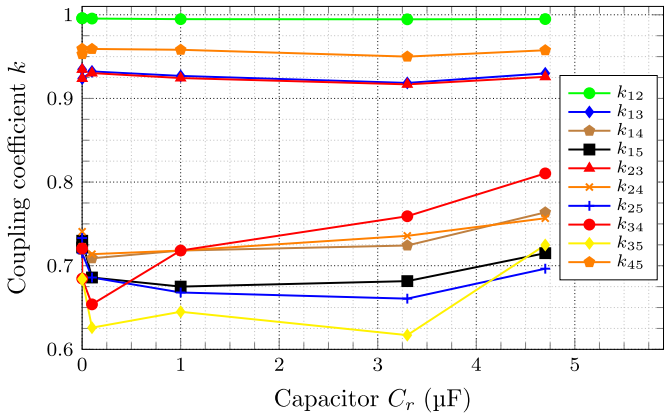

Fig. 13. Influence of C_r in all ten coupling coefficients of matrix (36).

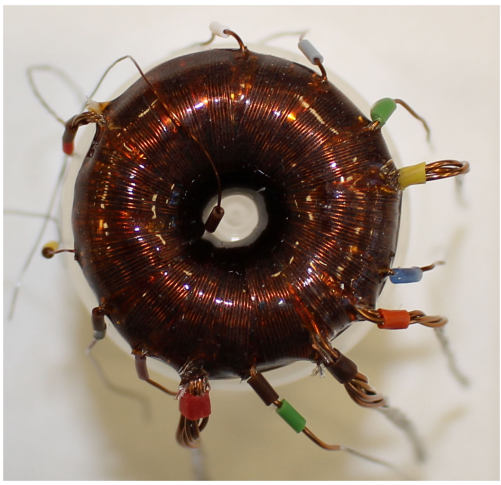

Fig. 14. Seven windings coupled inductor on an MPP toroidal core.

Fig. 13 clearly shows that the coupling coefficient k almost does not change with the frequency, except for low values of C_r, where the influence of $C_{\text{total parasitics}}$ begins to affect the measurement. As expected, low values of k are also very sensitive to the value of C_r, both due to the limit imposed by ξ_1 and ξ_2 and other parasitic elements, like R_{11} and R_{22} [see (32)] and the increase of the error factor itself for lower values of k [see (36)].

B. Seven Windings on MPP Toroid

The second magnetic element consists on a toroidal core (Magnetics 55348-A2), which has seven windings all tightly wound together (all coupling coefficients are close to one). A picture is shown in Fig. 14. The turns' ratio is given by (37).

Both methodologies (DiC and RE) have been applied to measure the inductance matrix of this coupled inductor. The capacitor used for the RE method is $C_r = 470\,\text{nF}$, having a lower limit of $C_{r\,\text{min}} = 7\,\text{nF}$ and an upper limit of $C_{r\,\text{max}} = 124\ \mu\text{F}$ [based on (32)]. The frequency chosen for the DiC method was 100 kHz .

Both measured matrices correspond to high coupling coefficients, as expected, but only the RE inductance matrix is PSD. The DiC measured matrix has even some physically wrong k values ($k > 1$)

$$n = \begin{pmatrix} 1 & 0.50 & 0.50 & 0.22 & 0.22 & 0.22 & 0.06 \\ 0.50 & 1 & 1.00 & 0.50 & 0.50 & 0.50 & 0.11 \\ 0.50 & 1.00 & 1 & 0.50 & 0.50 & 0.50 & 0.11 \\ 0.22 & 0.50 & 0.50 & 1 & 1.00 & 1.00 & 0.26 \\ 0.22 & 0.50 & 0.50 & 1.00 & 1 & 1.00 & 0.26 \\ 0.22 & 0.50 & 0.50 & 1.00 & 1.00 & 1 & 0.26 \\ 0.06 & 0.11 & 0.11 & 0.26 & 0.26 & 0.26 & 1 \end{pmatrix} \tag{37}$$

$$k_{\text{DiC}} = \begin{pmatrix} 1 & 0.984 & 0.984 & 0.984 & 0.983 & 0.967 & 0.885 \\ 0.984 & 1 & 0.997 & 0.998 & 0.996 & 0.982 & 0.950 \\ 0.984 & 0.997 & 1 & 0.996 & 0.996 & 0.982 & 0.951 \\ 0.984 & 0.998 & 0.996 & 1 & 1.005 & 0.984 & 0.977 \\ 0.983 & 0.996 & 0.996 & 1.005 & 1 & 0.984 & 0.968 \\ 0.967 & 0.982 & 0.982 & 0.984 & 0.984 & 1 & 1.033 \\ 0.885 & 0.950 & 0.951 & 0.977 & 0.968 & 1.033 & 1 \end{pmatrix} \tag{38}$$

$$k_{\text{RE}} = \begin{pmatrix} 1 & 0.993 & 0.990 & 0.979 & 0.971 & 0.985 & 0.990 \\ 0.993 & 1 & 0.991 & 0.983 & 0.969 & 0.987 & 0.993 \\ 0.99 & 0.991 & 1 & 0.972 & 0.983 & 0.987 & 0.990 \\ 0.979 & 0.983 & 0.972 & 1 & 0.973 & 0.967 & 0.980 \\ 0.971 & 0.969 & 0.983 & 0.973 & 1 & 0.975 & 0.974 \\ 0.985 & 0.987 & 0.987 & 0.967 & 0.975 & 1 & 0.984 \\ 0.990 & 0.993 & 0.990 & 0.980 & 0.974 & 0.984 & 1 \end{pmatrix}. \tag{39}$$

Therefore, this experiment demonstrates that magnetic elements with high coupling coefficient are better measured with the RE method. The influence of the turns' ratio can also be appreciated on the low values measured in this case with the DiC method.

To check how the frequency affects the RE method, all the coupling coefficients have been measured with several resonant capacitors C_r.

Fig. 15 clearly shows that the coupling coefficient k does almost not change with the frequency, except for low values of C_r, where the influence of $C_{\text{total parasitics}}$ begins to affect the measurement.

C. Three Windings on E-type Laminated-Iron Core

Finally, a three-phase grid filter inductor of 2 mH , 10 A, where all windings have the same turns' ratio, has been measured. The capacitor used for the RE method is $C_r = 10\ \mu\text{F}$,

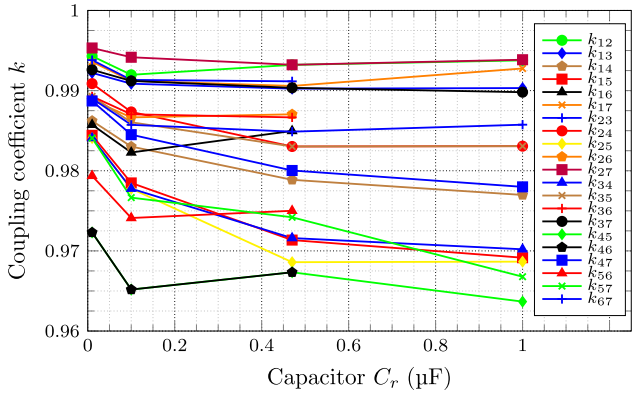

Fig. 15. Influence of C_r in all twenty one coupling coefficients of matrix (39).

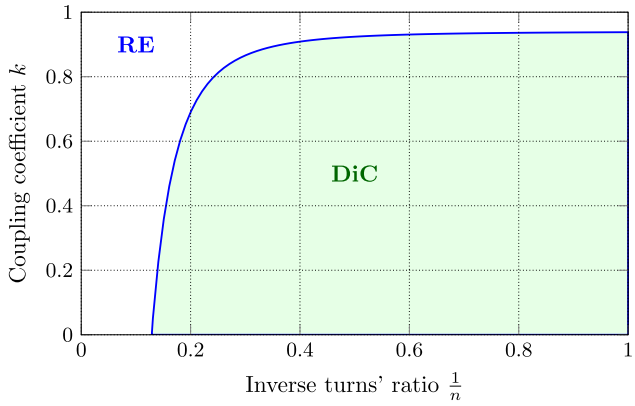

Fig. 16. Applicability of the new presented RE and the known DiC method depending on the turns' ratio n and the coupling coefficient k to measure coupling coefficient and mutual inductance.

having a lower limit of $C_{r\,\text{min}} = 112$ pF and an upper limit of $C_{r\,\text{max}} = 1$ mF [see (32)]. The frequency chosen for the DiC method was 100 Hz.

Both methods (DiC and RE) have also been applied to this inductor. The resulting matrices, for both methods, are PSD,

The coupling coefficient matrices measured for both cases are

$$k_{\text{DiC}} = \begin{pmatrix} 1 & 0.575 & 0.315 \\ 0.575 & 1 & 0.576 \\ 0.315 & 0.576 & 1 \end{pmatrix} \tag{40}$$

$$k_{\text{RE}} = \begin{pmatrix} 1 & 0.628 & 0.612 \\ 0.628 & 1 & 0.629 \\ 0.612 & 0.629 & 1 \end{pmatrix}. \tag{41}$$

Equations (40) and (41) show two PSD matrices but with different elements. As already explained in Section IV, where this inductance was used as example, the FEA provides theoretical values [shown in (33)], that justify that (40) represents the correct coupling coefficient matrix.

This time, the experiment demonstrates that low coupling coefficient magnetic elements are better measured using the DiC method instead of the RE method, due to the loss of accuracy for low values of k when using the RE method.

D. Applicability Results

The presented experimental validation confirms the theoretical results discussed earlier. Thus, it can be concluded that both methods have to be used depending on the turns' ratio n and the coupling coefficient k of a windings' pair. The accuracy analysis found in Section II-A has shown that the turns' ratio plays an important role and dissimilar turns' number can increase the relative error of the DiC method very fast, independently of the coupling coefficient k. Due to physical and mechanical constraints, the DiC method can also be error prone and additional errors can add up if the coupling coefficient k is close to one. Finally, as explained in Section III-C, for values of k close to one, the relative error of the RE method is small as long as the other limitations analyzed are respected. Summarizing, the recommended areas of the application are shown in Fig. 16.

It has been demonstrated that the RE method provides a valid measurement where the DiC method has an unacceptable relative error. In addition, when coupling coefficient k becomes very large, the DiC method could also provide less accurate results compared to the RE method, although in this case the error depends on the measurement technique and the core material (mainly iron powder and soft ferrites). Anyhow, under this condition, the RE method will have higher accuracy and should be the preferred option.

Taking into account that magnetic elements of dc/dc converters, which definitely is a very important application area in power electronics and in those cases that have high coupling coefficients k_{ij} the RE method could be considered the most accurate method to measure the coupling coefficient and mutual inductances matrices of multiwinding magnetic parts.

VI. Conclusion

This paper proposes a new method to measure coupling coefficients and mutual inductances for dissimilar turns' number or tightly coupled windings called RE. It allows to measure the inductance matrix, assuring that the resulting matrix is PSD under conditions where other methods fail.

The RE method is compared to the DiC method and its application range has been established. In fact, the RE method should be applied to windings with dissimilar turns' number or high coupling coefficient k, where the DiC method does not provide accurate results. It is recommended to apply the RE method for turns' ratio $1/n < 0.2$ and coupling coefficient between a pair of windings larger than $k \gtrsim 0.95$. For coupling coefficient lower than $k \lesssim 0.95$, the DiC method should be used. These values are approximate and depend also on the measurement instrument accuracy and physical and mechanical constraints. This paper also shows how the FEA confirms the measured values for a three-phase inductor.

The influence of losses and parasitic capacitance of the magnetic element when applying the RE method to measure its

inductance matrix has also been studied in a normalized manner, using normalized frequency s_n, the damping factors ξ_1, ξ_2, and ξ_{12} and the normalized impedance $|Z_{\text{norm}}|$. The normalized study allows us to determine the influence of the resistance together with the chosen resonance capacitor and the inductance value. The range of the resonance capacitor to be used in the RE method has been established.

ACKNOWLEDGMENT

The authors would like to thank Prof. W. G. Hurley and Dr. Duffy of the Power Electronics Research Centre at the National University of Ireland, Galway, for their help with the results in Section IV. The authors would also like to thank Mr. D. Osorno for his help in the lab and Mr. J. L. Gasent-Blesa for his support.

REFERENCES

[1] Y. T. Chen, Z. X. Lu, and R. H. Liang, "Analysis and design of a novel high-step-up dc/dc converter with coupled inductors," *IEEE Trans. Power Electron.*, vol. 33, no. 1, pp. 425–436, Jan. 2017.

[2] A. Shaltout, M. Lipski, and S. Gregori, "Analysis of boost dc-dc converters with integrated coupled inductors," in *Proc. 28th Int. Conf. Microelectron.*, Dec. 2016, pp. 129–132.

[3] O. Kircioğlu, M. Ünlü, and S. Çamur, "Modeling and analysis of dc-dc sepic converter with coupled inductors," in *Proc. Int. Symp. Ind. Electron.*, Nov. 2016, pp. 1–5.

[4] X. Huang, F. C. Lee, Q. Li, and W. Du, "High-frequency high-efficiency GAN-based interleaved CRM bidirectional buck/boost converter with inverse coupled inductor," *IEEE Trans. Power Electron.*, vol. 31, no. 6, pp. 4343–4352, Jun. 2016.

[5] D. Ebisumoto *et al.*, "Design of a four-phase interleaved boost circuit with closed-coupled inductors," in *Proc. IEEE Energy Convers. Congr. Expo.*, Sep. 2016, pp. 1–6.

[6] D. Maksimovic, R. W. Erickson, and C. Griesbach, "Modeling of cross-regulation in converters containing coupled inductors," *IEEE Trans. Power Electron.*, vol. 15, no. 4, pp. 607–615, Jul. 2000.

[7] G. W. Ludwig and S. A. El-Hamamsy, "Coupled inductance and reluctance models of magnetic components," *IEEE Trans. Power Electron.*, vol. 6, no. 2, pp. 240–250, Apr. 1991.

[8] W. G. Hurley, D. J. Wilcox, and P. S. McNamara, "Calculation of short circuit impedance and leakage impedance in transformer windings," in *Proc. 22nd Annu. Power Electron. Spec. Conf.*, Jun. 1991, pp. 651–658.

[9] B. Cogiore, J. P. Keradec, and J. Barbaroux, "The two winding ferrite core transformer: An experimental method to obtain a wide frequency range equivalent circuit," in *Proc. IEEE Instrument. Meas. Technol. Conf.*, May 1993, pp. 558–562.

[10] A. Dauhajre and R. D. Middlebrook, "Modelling and estimation of leakage phenomena in magnetic circuits," in *Proc. 17th Annu. IEEE Power Electron. Speci. Conf.*, Jun. 1986, pp. 213–226.

[11] X. Margueron and J. P. Keradec, "Design of equivalent circuits and characterization strategy for n-input coupled inductors," *IEEE Trans. Ind. Appl.*, vol. 43, no. 1, pp. 14–22, Jan. 2007.

[12] J. Zhang, Z. Ouyang, M. C. Duffy, M. A. E. Andersen, and W. G. Hurley, "Leakage inductance calculation for planar transformers with a magnetic shunt," *IEEE Trans. Ind. Appl.*, vol. 50, no. 6, pp. 4107–4112, Nov. 2014.

[13] Z. Ouyang, J. Zhang, and W. G. Hurley, "Calculation of leakage inductance for high-frequency transformers," *IEEE Trans. Power Electron.*, vol. 30, no. 10, pp. 5769–5775, Oct. 2015.

[14] W. G. Hurley and M. C. Duffy, "Calculation of self- and mutual impedances in planar sandwich inductors," *IEEE Trans. Mag.*, vol. 33, no. 3, pp. 2282–2290, May 1997.

[15] J. P. Keradec, B. Cogitore, and F. Blache, "Power transfer in a two-winding transformer: from 1-D propagation to an equivalent circuit," *IEEE Trans. Mag.*, vol. 32, no. 1, pp. 274–280, Jan. 1996.

[16] A. Pietkiewicz and D. Tollik, "Coupled-inductor current-doubler topology in phase-shifted full-bridge dc-dc converter," in *Proc. 20th Int. Telecommun. Energy Conf.*, 1998, pp. 41–48.

[17] Y. Tokad and M. B. Reed, "Criteria and tests for readability of the inductance matrix," *Trans. Amer. Inst. Electric. Eng., Part I, Commun. Electron.*, vol. 78, no. 6, pp. 924–926, Jan. 1960.

[18] X. Liu and S. Y. R. Hui, "Equivalent circuit modeling of a multilayer planar winding array structure for use in a universal contactless battery charging platform," *IEEE Trans. Power Electron.*, vol. 22, no. 1, pp. 21–29, Jan. 2007.

[19] Y. P. Su, X. Liu, and S. Y. R. Hui, "Mutual inductance calculation of movable planar coils on parallel surfaces," *IEEE Trans. Power Electron.*, vol. 24, no. 4, pp. 1115–1123, Apr. 2009.

[20] J. G. Hayes, N. O'Donovan, M. G. Egan, and T. O'Donnell, "Inductance characterization of high-leakage transformers," in *Proc. 18th Annu. Appl. Power Electron. Conf. Expo.*, Feb. 2003, vol. 2, pp. 1150–1156

[21] K. V. Kantak, "Coupled inductor characterization and spice modeling," in *Proc. 5th Annu. Proc. Appl. Power Electron. Conf. Expo.*, Mar. 1990, pp. 330–335.

[22] C. McLyman, *Transformer and Inductor Design Handbook*, 4th ed. Boca Raton, FL, USA: CRC Press, 2016.

[23] C. R. Sullivan, "Computationally efficient winding loss calculation with multiple windings, arbitrary waveforms, and two-dimensional or three-dimensional field geometry," *IEEE Trans. Power Electron.*, vol. 16, no. 1, pp. 142–150, Jan. 2001.

[24] B. X. Foo, A. L. F. Stein, and C. R. Sullivan, "A step-by-step guide to extracting winding resistance from an impedance measurement," in *Proc. IEEE Appl. Power Electron. Conf. Expo.*, Mar. 2017, pp. 861–867.

David Gilabert-Palmer received the B.Sc. and M.Sc. degrees in electronic engineering in 2014 from the University of Valencia, Valencia, Spain, where he is currently working toward the Ph.D. degree on complex coupled inductors.

He is also a member of the Laboratory of Industrial Electronics and Instrumentation. His research interests include high-frequency magnetics, coupled inductors, and space power electronics.

Esteban Sanchis-Kilders (M'00–SM'14) was born in Valencia, Spain, in 1967. He received the M.Sc. degree in physics, with specialization in electronics, and the Ph.D. degree from the University of Valencia, Valencia, Spain, in 1990 and 1997, respectively.

His employment experience includes one year with GH Industrial S.A. and two years with the Power Conditioning Section, European Space Agency, Noordwijk, The Netherlands. Since 1997, he has been with the University of Valencia, where he has been a Full Professor since 2016. He is also a member of the Laboratory of Industrial Electronics and Instrumentation. His main research interests include space power electronics, magnetism control, and industrial applications.

Vicente Esteve (M'03–SM'14) was born in Valencia, Spain, in 1961. He received the M.Sc. and Ph.D. degrees from the University of Valencia, Spain, in 1986 and 1999, respectively.

He is currently an Associate Professor with the University of Valencia and is a member of the Laboratory of Industrial Electronics and Instrumentation. He is a Consultant of several electronics companies in the field of power supplies and advanced topologies. His research activities include high-frequency rectifiers and inverters for industrial applications, high-power inverters for induction heating, and electronic instrumentation.

Agustín Ferreres was born in Sant Mateu, Spain, in 1963. He received the M.Sc. degree in physics with specialization in electronics and the Ph.D. degree in electronic engineering from the University of Valencia, Spain, in 1993 and 1999, respectively.

For two years, he was a Power Electronics Researcher with the R+D Department of GH Industrial S.A. In 1995, he was with the Laboratory of Industrial Electronics and Instrumentation, University of Valencia, where he is currently an Associate Professor. His research interests include space power electronics and industrial applications.

Juan B. Ejea was born in Xàtiva, Spain, in 1969. He received the M.Sc. degree in physics, with specialization in electronics, and the Ph.D. degree in electronic engineering from the University of Valencia, Spain, in 1993 and 2000, respectively.

His employment experience includes two years with GH Industrial S.A., two years with the Power Section of the European Laboratory for Particle Physics, Geneva, Switzerland. Since 1995, he has been with the University of Valencia, where he is currently an Associate Professor. He is also a member of the Laboratory of Industrial Electronics and Instrumentation. His main research interests include space power systems and industrial applications.

Enrique Maset (M'00) was born in Xàtiva, Spain, in October 1965. He received the M.Sc. and Ph.D. degrees in physics from the University of Valencia, Spain, in 1988 and 1993, respectively.

He is currently an Associate Professor with the Department of Electronic Engineering, University of Valencia, where he is also a member of the Laboratory of Industrial Electronics and Instrumentation. His main research interests include space power electronics and static and dynamic characterization of electronic power devices.

José Jordán (M'08–SM'15) was born in 1964. He received the M.Sc. degree in physics with specialization in electronics and the Ph.D. degree in electronic engineering from the University of Valencia, Spain, in 1989 and 2003, respectively.

From 1987 to 2001, he held research positions at GH Electrotermia, where his activities were focused on the design of high-frequency and high-power converters. He is currently an Associate Professor with the University of Valencia, where he is a member of the Laboratory of Industrial Electronics and Instrumentation. His research interests include power semiconductor characterization and power converters. In these areas, he also works as a Consultant for industry.

Enrique Dede received the Ph.D. degree in electronics from the University of Valencia, Valencia, Spain.

Since 1991, he has been a Full Professor in power Electronics, University of Valencia, where he founded the Laboratory of Industrial Electronics and Instrumentation. He was a Principal R&D Advisor with the company GH Electrotermia S.A. He holds several international patents on high frequency inverters for induction heating and has authored or coauthored more than 200 papers in the field of power electronics. He has been a member of the European Working Group of the IAS-IEEE, is nowadays member of the International Advisory Board of the PCIM-Europe and a member of the Board of Directors of PCIM-Asia. He was the President of the joint Spanish IEEE Chapter of the Power Electronics and Industrial Electronics Society. He is currently the Vice-President of the European Power Electronics Association.